BCAT1 is a NOTCH1 target and sustains the oncogenic function of NOTCH1

Valeria Tosello,[1*] Ludovica Di Martino,[2*] Adonia E. Papathanassiu,[3] Silvia Dalla Santa,[2] Marco Pizzi,[4] Lara Mussolin,[5] Jingjing Liu,[6] Pieter van Vlierberghe[7†] and Erich Piovan[2,8]

[1]Basic and Translational Oncology Unit, Veneto Institute of Oncology IOV-IRCCS, Padua, Italy; [2]Department of Surgery, Oncology and Gastroenterology, University of Padua, Padua, Italy; [3]Ergon Pharmaceuticals, LLC, Washington DC, USA; [4]Surgical Pathology and Cytopathology Unit, Department of Medicine - DIMED, University of Padua, Padua, Italy; [5]Unit of Onco-hematology, Stem Cell Transplant and Gene Therapy, Department of Women's and Children's Health, University of Padua, Padua, Italy; [6]Department of Computational Biology, St. Jude Children's Research Hospital, Memphis, TN, USA; [7]Department of Biomolecular Medicine, Ghent University, Ghent, Belgium and [8]Immunology and Molecular Oncology Unit, Veneto Institute of Oncology IOV-IRCCS, Padua, Italy

VT and LDM contributed equally as first authors.

†*Posthumously.*

Correspondence: E. Piovan
erich.piovan@unipd.it

Received: March 29, 2024.
Accepted: August 23, 2024.
Early view: September 5, 2024.

https://doi.org/10.3324/haematol.2024.285552

Abstract

High levels of branched-chain amino acid (BCAA) transaminase 1 (BCAT1) have been associated with tumor aggressiveness and drug resistance in several cancer types. Nevertheless, the mechanistic role of BCAT1 in T-cell acute lymphoblastic leukemia (T-ALL) remains uncertain. We provide evidence that Bcat1 was over-expressed following NOTCH1-induced transformation of leukemic progenitors and that NOTCH1 directly controlled BCAT1 expression by binding to a BCAT1 promoter. Further, using a *NOTCH1* gain-of-function retroviral model of T-ALL, mouse cells genetically deficient for *Bcat1* showed defects in developing leukemia. In murine T-ALL cells, Bcat1 depletion or inhibition redirected leucine metabolism towards production of 3-hydroxy butyrate (3-HB), an endogenous histone deacetylase inhibitor. Consistently, BCAT1-depleted cells showed altered protein acetylation levels which correlated with a pronounced sensitivity to DNA damaging agents. In human NOTCH1-dependent leukemias, high expression levels of BCAT1 may predispose to worse prognosis. Therapeutically, BCAT1 inhibition specifically synergized with etoposide to eliminate tumors in patient-derived xenograft models suggesting that BCAT1 inhibitors may have a part to play in salvage protocols for refractory T-ALL.

Introduction

T-cell acute lymphoblastic leukemia (T-ALL) is an aggressive hematological cancer accounting for approximately 15% of pediatric and approximately 25% of adult ALL cases, requiring intensive chemotherapy regimens.[1,2] Notwithstanding improved cure rates, especially in pediatric cases, a significant fraction of patients (~15%) relapse. Children and adults with relapsed T-ALL face poor prognosis due to low remission rates and increased morbidity and mortality with salvage therapy. There is no doubt that more effective treatment strategies are needed, especially for refractory T-ALL. It is generally accepted that T-ALL is a heterogeneous disease, the result of a wide spectrum of genetic lesions and environmental cues that cooperate to promote leukemogenesis[3,4] leading to the aberrant growth of immature T-cell progenitors. Gain-of-function mutations in *NOTCH1* are among the most common genetic alterations found in T-ALL.[5] NOTCH1 plays an important physiological role in promoting T-cell lineage and cell growth during thymic development. Its activation following ligand binding requires proteolytic cleavage by γ-secretase-containing protease complexes as well as translocation of the cleaved NOTCH1 intracellular domain (NICD) to the nucleus to facilitate the transcription of numerous downstream targets.[6] *NOTCH1* gain-of function mutations (mutNOTCH1) in T-ALL determine the activation of NOTCH1 in the absence of a ligand and/or prevent termination of NOTCH1 signaling in the nucleus. Constitutive NOTCH1 signaling in T-ALL is linked to the transcriptional activation of numerous anabolic pathways involved in cell growth such as ribosome biosynthesis, protein translation and nucleotide and ami-

no acid metabolism.[7,8] In addition to its transcriptional activities, NOTCH1 is a direct, negative regulator of DNA damage response (DDR) through binding and inhibiting of the ATM (ataxia-telangiectasia mutated) Ser/Thr kinase.[9] This links *NOTCH1* activation to the high number of genetic alterations found in T-ALL, which are thought to be driven by errant DNA repair.

The present study reports that, in addition to its direct effect on the HR pathway, mutNOTCH1 indirectly regulates DDR by upregulating BCAT1. Specifically, we found that BCAT1 was a transcriptional target of mutNOTCH1, which was expressed early in the process of leukemogenesis and shown to regulate not only branched chain amino acid (BCAA) levels but also ketone body synthesis (3-hydroxybutyrate, 3-HB). 3-HB accumulation in BCAT1-deficient cells modified protein acetylation levels and altered DDR resulting in accentuated DNA damage and cell death, especially when combined with a genotoxic insult. The increased chemosensitivity to double strand break (DSB)-inducing agents, observed in T-ALL models following BCAT1 inhibition, suggests that BCAT1 is a novel therapeutic target in T-ALL.

Methods

Western blotting

Total cell lysates were prepared using RIPA lysis buffer supplemented with phosphatase inhibitor cocktail set I and II (Sigma-Aldrich, Merck, Darmstadt, Germany) and protease inhibitor cocktail tablets (Roche, Burgess Hill, UK) and normalized for protein concentration using the BCA method (Pierce, Pero, Italy). For western blotting, protein samples were separated on 4-12% gradient Tris-glycine or 3-8% Tris-acetate SDS-PAGE gels (Invitrogen, Waltham, MA, USA) and transferred to PVDF membrane (Millipore, Billerica, MA, USA). Antibodies against tubulin (TU-02), MYC and p53 (DO-1) were from Santa Cruz Biotechnology (Dallas, TX, USA); antibodies recognizing cleaved NOTCH-1 (ICN1; Val 1744), β-actin, p21, BCAT2, BCAT1, Ku80, Ku70, histone H3, cleaved PARP-1, cleaved caspase 3, phosphorylated H2AX (pS139), phosphorylated DNA-PKcs (pS2056), total DNA-PKcs, phosphorylated ATM (pS1981), total ATM, phosphorylated CHK2 (pT68), total CHK2, phosphorylated TP53 (pS15), acetylated p53 (K382) and GADPH were from Cell Signaling Technology (Danvers, MA, USA). Acetyl-Histone H3 Antibody Sampler Kit (#9927) was also from Cell Signaling Technology. Mouse anti-BCAT1 (BD Pharmingen, Oxford, UK) was also used. The BioRad ChemiDoc XRS Imager was used to capture the signals from the blots.

Chromatin immunoprecipitation quantitative polymerase chain reaction

Chromatin immunoprecipitation (ChIP) assays were performed using the SimpleChIP plus Enzymatic Chromatin IP kit (Cell Signaling Technology, #9005) following the manufacter's protocol. Briefly, 4 x10^6 cells were fixed with formaldehyde in a final concentration of 1% for 10 minutes at room temperature. The crosslinking reaction was quenched with a 5 M glycine solution, and the cells were then centrifuged, washed twice with ice-cold phosphate-buffered saline (PBS) and lysed. Cell nuclei were prepared and chromatin was digested with micrococcal nuclease, then sonicated. The sheared chromatin was immunoprecipitated with human Notch-1 intracellular domain antibody (R&D Systems, Minneapolis, MN; Cat#AF3647). Normal sheep immunoglobulin G (IgG) (Cat#5-001-A, R&D Systems) was used as a non-specific antibody control for immunoprecipitation. Following an overnight incubation with antibodies, 30 µl of protein G magnetic beads was added at 4°C for 2 hours (h). Beads were washed, and chromatin was eluted. Crosslinks were reverted according to kit instructions. The DNA was purified using DNA purification buffers and spin columns (Cell Signaling Technology #14209) following kit instructions. The immunoprecipitated DNA was subjected to real-time polymerase chain reaction (PCR) reaction using ChIP primer sets (listed in *Online Supplementary Table S1*), which were designed to include the promoter and negative regions of the *BCAT1* gene. *HES1* promoter region was used as positive control. Fold enrichment was calculated as a ratio of amplification efficiency of ChIP sample over that of the IgG. More specifically, the amplification efficiency (AE) of each primer set was used to determine the amplification efficiency of the ChIP sample and the IgG sample as follows: % ChIP = AE (Input Ct – ChIP Ct) x (dilution factor; Fd)(100); % IgG = AE (Input Ct - IgG Ct) x (Fd)(100); fold enrichment =% ChIP/% IgG.

Statistical analyses

Results were expressed as mean value ± standard deviation (SD). Student's *t* test and non-parametric *t* test (Mann-Whitney) were used where appropriate. A non-parametric test (Fisher's exact test) was used to compare qualitative data. The Kaplan-Meier method was used to estimate the distributions of overall survival (OS). OS was considered as the time from diagnosis to date of death. The log-rank test was used to compare survival distributions. All statistical tests were two-sided, unpaired and $P<0.05$ was considered statistically significant ($^{*}P<0.05$, $^{**}P<0.01$, $^{***}P<0.001$). Analysis of drugs' interaction was performed using Combenefit software.[10] The sample size for animal xenograft experiments was determined on the basis of prior studies that yielded a two-tailed statistical test with apprximately 80% power to detect a 2-fold change in tumor burden (α=0.05). All attempts at replication were consistent for all animal and cell culture experiments.

Mouse experiments

The study was approved by the Institutional Review Board (OPBA) of the University of Padova (protocol code 238591; 25 June 2019) and the Italian Ministry of Health (DGSAF

0006112; 177/2020-PR; 10/03/2020).

Information on cell lines and primary leukemia samples, mouse transplantation experiments and studies, flow cytometry and analysis of T-cell distribution, quantitative real-time PCR, total histone extraction, immunohistochemistry, immunoprecipitation of acetylated proteins, neutral comet assay, analysis of publicly available datasets, RNA sequencing and gene-set enrichment analysis, steady state metabolite profiling, stable-isotope tracing experiments, analysis of ChIP-sequencing databases, cell viability assays and flow cytometry, plasmids, lentiviral constructs and viral production, luciferase reporter experiments, methylation specific PCR (MSP) methods are detailed in the *Online Supplementary Appendix*.

Results

NOTCH1 upregulates BCAT1 expression in *NOTCH1*-mutated human T-cell acute lymphoblastic leukemia by binding to a *BCAT1* promoter

In order to understand the role that BCAT1 plays in T-ALL development, we analyzed gene expression data from a NOTCH1-induced murine T-ALL (NIC) model. In that model, overexpression of an activated, intracellular form of Notch1 (*ICN1*) in transplanted Lin-negative murine hematopoietic cells leads to the development of an abnormal $CD4^+CD8^+$ double positive (DP) T-cell subset at 2 weeks of transplantation followed by the rise of a highly tumorigenic DP leukemic population at 6-8 weeks of transplantation[11,12] In the gene set of Figure 1A, *Bcat1* was highly upregulated in leukemic DP cells compared to normal DP cells. The increase in Bcat1 expression occurred early in T-ALL development as evident from the heat map of *Online Supplementary Figure S1A*, and was unique among other enzymes involved in BCAA metabolism (e.g., Bcat2, Bckdha, and Bckdhb), whose expression did not exhibit a specific pattern (*Online Supplementary Figure S1A*). To confirm the above observations, we compared transcript and protein levels of Bcat1 and Bcat2 in thymocytes isolated from normal C57/BL6 mice and leukemic cells obtained from spleens of mice bearing T-ALL tumors. The tumors were induced through overexpression of an activated form of *NOTCH1* lacking a major portion of the extracellular domain (Δ*E-NOTCH1*). As in the case of the NIC model, the development of leukemia in the Δ*E-NOTCH1* model (NOTCH1-T tumors) was associated with increased Bcat1 levels (Figure 1B). On the other hand, the gene expression of *Bcat2*, the mitochondrial isoform of BCAT, was not consistently altered with the development of leukemia, although a decrease was observed in the protein levels in NOTCH1-T tumors (*Online Supplementary Figure S1B, C*). The results suggest that the expression of Bcat1 and Bcat2 in NOTCH1-T tumors may be anti-correlated. Since Bcat1 and Bcat2 are metabolic enzymes, we attempted to identify a leukemia-specific metabolic signature by extracting metabolites from NOTCH1-T tumors (N=3) and murine thymic tissue (N=3). We quantified 112 metabolites by using a highly sensitive capillary electrophoresis-time-of-flight mass spectrometry (CE-TOFMS) and capillary electrophoresis-tandem mass spectrometry (CE-MS/MS) (*Online Supplementary Figure S1D*). While thymic tissue preferentially expressed metabolites associated with lipid oxidation (e.g., carnitine and citric acid) as well as purine and pyrimidine metabolism, metabolites found elevated in NOTCH1-T tumors were linked to glycolysis (lactic acid) and tricarboxylic acid (TCA) cycle replenishment (succinic, fumaric, and malic acids) indicating a significant metabolic shift with development of leukemia (*Online Supplementary Figure S1E*). This metabolic feature was maintained when heavily infiltrated thymuses were used as a source of leukemia (*Online Supplementary Figure S2A*). NOTCH1-T tumors were also characterized by increased concentrations of BCAA (*Online Supplementary Figures S1F, S2B*). While BCAA biosynthesis was identified as a significantly enriched pathway in NOTCH1-T tumors by metabolite set enrichment analysis (*Online Supplementary Figure S1E*), active uptake could not be excluded as the tumors showed increased expression of the neutral amino acid transporter *slc7a5* (LAT1) compared to normal thymic tissues (*Online Supplementary Figure S1G*).

In order to determine if BCAT1 overexpression is also a characteristic of human T-ALL, we utilized a publicly available dataset, which profiled both normal human thymocyte populations and bone marrow samples of childhood T-ALL patients at the time of diagnosis.[13] We found that BCAT1 was highly expressed in numerous T-ALL samples (*Online Supplementary Figure S1H*). To confirm that human T-ALL is indeed linked to increased BCAT1 expression, we used a comprehensive microarray data set[14,15] consisting of T-ALL patients (N=57) and thymocyte subsets (7 thymocyte and mature T-cell subsets derived from 3 independent donors). BCAT1 expression was again found to be significantly upregulated in a fraction of T-ALL specimens compared to thymocyte subsets (Figure 1C). T-ALL can be subclassified into three differentiation stages based on cluster of differentiation (CD) surface markers, such as early/precortical, cortical, and mature/postcortical. To identify patient groups with upregulated BCAT1 expression, we utilized a well-characterized T-ALL gene dataset (TARGET cohort), obtained from 264 pediatric T-ALL patients.[16] We found *BCAT1* to be preferentially expressed in the cortical (CD1a-positive) T-ALL immunophenotypical subgroup (*Online Supplementary Figure S1I*). Since *NOTCH1* activating mutations are highly prevalent in the cortical subgroup,[3] we hypothesized that NOTCH1 regulates BCAT1 expression. Subdividing the TARGET cohort of patients into *NOTCH1/FBXW7*-mutated and *NOTCH1/FBXW7* wild-type disclosed that the former had higher BCAT1 levels compared to *NOTCH1* wild-type patients (*Online Supplementary Figure S1J*). This observation was confirmed in two independent T-ALL cohorts

composed of 37 diagnostic pediatric samples included in the Children's Oncology Group P9404 study[17] and 130 pediatric and adult samples from the Shanghai Institute of Hematology project with known *NOTCH1* mutational status (*Online Supplementary Figure S1K, L*).[18] We then analyzed BCAT1 expression in a comprehensive panel of T-ALL cell lines. *Online Supplementary Figure S1M* discloses a heterogeneous pattern of BCAT1 protein expression, which was not evidently correlated with the mutational status of NOTCH1, as detected by the presence of ICN1, although BCAT1 transcript expression did correlate with HES1 expression (*Online Supplementary Figure S1N*). *HES1* gene is a well-known NOTCH1-target gene. We also evaluated the methylation status of *BCAT1* promoter in a cell line panel and determined that gene methylation status controlled BCAT1 expression in a particular cell line (*Online Supplementary Figure S1O, P*). We also analyzed the transcript and protein levels (Figure 1D) of BCAT1 in previously generated patient-derived xenografts (PDX).[19,20] PDX samples possessing activated NOTCH1 (*NOTCH1/FBXW7* mutant/NICD1-positive cases) showed higher BCAT1 levels compared to NICD1-negative cases (Figure 1D). Finally, we evaluated BCAT1 and HES1 expression levels using immunohistochemistry in primary T-cell lymphoblastic leukemia/lymphoma (T-ALL/T-LBL; N=10), PDX samples (N=10) and normal human thymuses (N=3). We found weak expression of all three markers in normal thymus (*Online Supplementary Figure S3A*). The staining pattern for BCAT1 and HES1 was rather heterogeneous in leukemia samples (*Online Supplementary Figure S3B, C*), however we found a statistically significant association between BCAT1 expression and HES1 staining (Fisher's exact test $P<0.05$; *Online Supplementary Figure S3C*). We used HES1 staining as a surrogate for NOTCH1 activation status as Sanger-based sequencing of *NOTCH1* and *FBXW7* genes from formalin-fixed parafin-embedded material failed in most patient cases. On the other hand, we found no association between BCAT2 and HES1 staining (*Online Supplementary Figure S3D*). These results further suggest that NOTCH1-activated leukemia cases express higher levels of BCAT1. Based on the above evidence, we hypothesized that NOTCH1 activation leads to BCAT1 overexpression.

In order to additionally evaluate whether BCAT1 represents a novel NOTCH1 downstream target gene, we treated NOTCH1-T tumor-bearing mice (5 independent tumors) with the γ-secretase inhibitor dibenzazepine (DBZ) and subjected vehicle-control (dimethyl sulfoxide [DMSO]) and treated (DBZ) tumors to transcriptomic analysis. We found that *Bcat1* gene expression was highly downregulated following *in vivo* NOTCH1 inhibition (*Online Supplementary Figure S4A*). Downregulation of *Bcat1* was also observed following similar analysis of *HDΔPEST NOTCH1* (*NOTCH1* mutant allele harboring both HD and PEST domain mutations) leukemias treated *ex vivo* with DBZ[21] (*data not shown*). Further, treatment of human *NOTCH1* mutant T-ALL cell lines (*in vitro*) and PDX samples (*in vivo*) with DBZ markedly reduced BCAT1 transcript and protein levels (Figure 1E; *Online Supplementary Figure S4B, C*). To determine whether NOTCH1 directly regulates BCAT1 expression in T-ALL, we analyzed deposited chromatin immunoprecipitation followed by next-generation sequencing (ChIP-sequencing) data of NOTCH1 chromatin binding sites in HPB-ALL cells, which are NOTCH1-mutant and MYC expressing T-ALL cells.[22] We found numerous NOTCH1 peaks in the BCAT1 locus; particularly prominent was a peak of approximately 0.5 kb near the BCAT1 transcription start site (TSS) (Figure 1F). In the vicinity of this peak region, a RBPJ site was found upstream of the TSS. To functionally characterize the potential role of this NOTCH1 binding region in *BCAT1* gene regulation, we inspected encyclopedia of DNA elements (ENCODE) data for epigenetic histone marks in this region in T-ALL cells. These analyses revealed *bona fide* promoter features associated with this region, including occupancy and high levels of DNA polymerase II (Pol II) and high levels of histone H3 Lys4 trimethylation (H3K4me3) (*Online Supplementary Figure S5*). Transposase-accessible chromatin with sequencing (ATAC-Seq) data also support an open chromatin state in this region (*Online Supplementary Figure S5*). Local ChIP experiments using specific primers centered around this region were performed in PF382 cells, which are NOTCH1 mutant and present modest levels of MYC protein expression (*Online Supplementary Figure S4C*). This analysis confirmed NOTCH1 binding in this area of the *BCAT1* promoter region (Figure 1F). Based on these results, we proposed that this NOTCH1- bound region could function as an important regulatory element driving BCAT1 expression in T-ALL cells. Consistent with that hypothesis, luciferase reporter assays in ICN1-transfected HEK 293T cells showed a dose-dependent activation of a reporter construct containing this approximately 0.5 kb region of the *BCAT1* promoter (including the upstream RBPJ binding site) (*Online Supplementary Figure S4D*). Reporter activity was severely reduced following mutation of the RBPJ binding site (*Online Supplementary Figure S4D*). Further, ICN1-induced reporter activity was progressively reduced using CB103, a highly selective and potent inhibitor of the CSL-NICD gene transcription complex[23] (*Online Supplementary Figure S4E*). On the other hand, knockdown of *MYC* or the use of *JQ1*[24] only modestly affected ICN1-induced reporter activity (*Online Supplementary Figure S4F, G*), strongly suggesting that MYC does not play a major role in regulating the activity of this region. Coherently, in HPB T-ALL cells (*Online Supplementary Figure S4H*), luciferase reporter assays showed strong activation of this *BCAT1* promoter reporter construct. Further, in HPB T-ALL cells reporter activity could progressively be reduced using CB103 (*Online Supplementary Figure S4I*) or following inactivation (deletion or mutation) of the RBPJ binding site, suggesting a prominent role for NOTCH1 in regulating reporter activity in T-ALL cells (*Online Supplementary Figure S4J*). This

notion was further strengthened by the observation that forced increased expression of ICN1 in HPB T-ALL cells augmented *BCAT1* promoter reporter activity but had very modest effects on the transcriptional activity of the *BCAT1* promoter construct having the RBPJ binding site mutated (*Online Supplementary Figure S4K*).

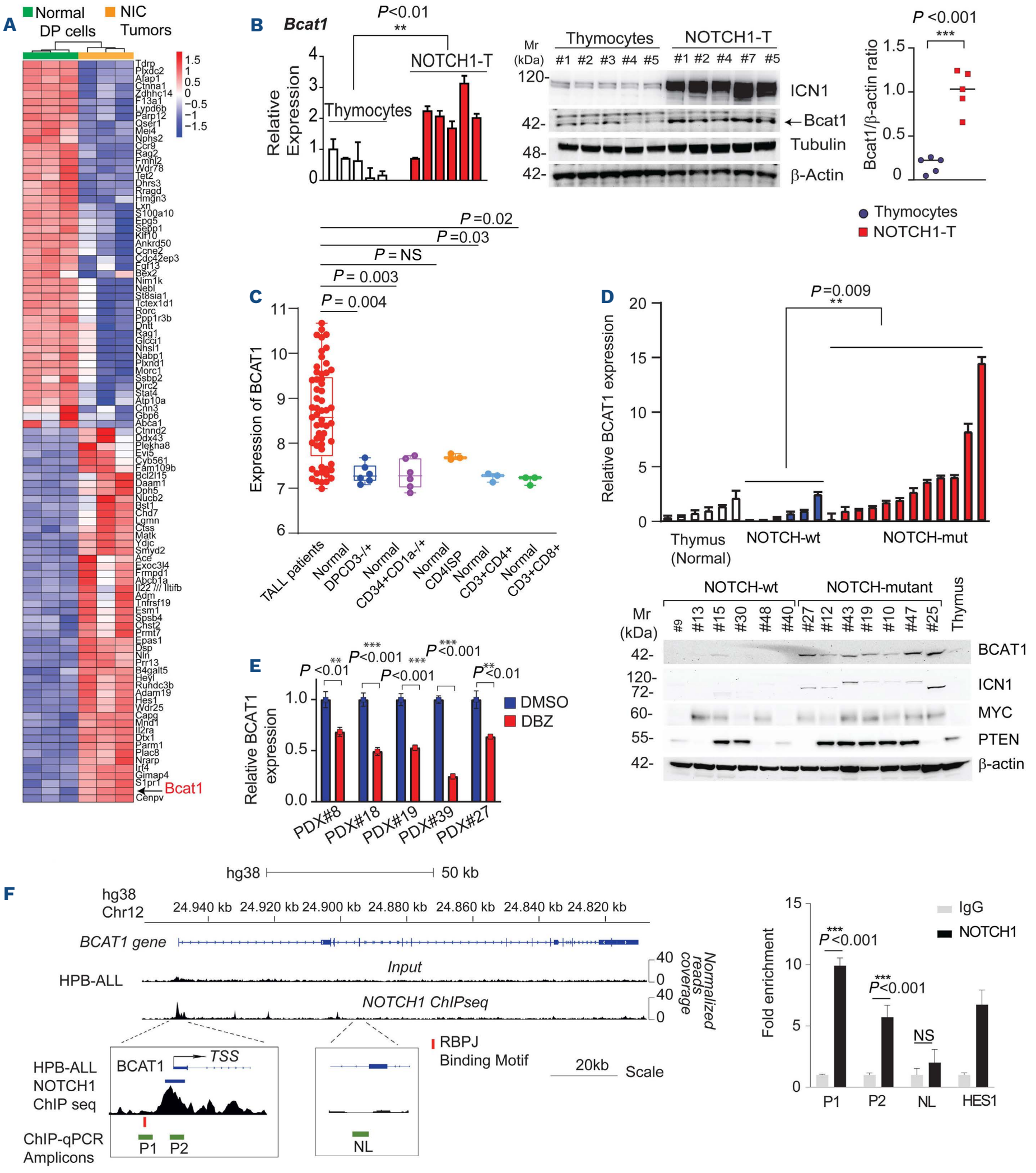

Continued on following page.

Figure 1. BCAT1 is upregulated during NOTCH1-dependent transformation. (A) Heat map showing the top 50 most downregulated and upregulated genes between normal double-positive (DP) cells and *ICN1*-induced DP leukemic cells (NIC Tumors). (B) Expression levels (quantitative polymerase chain reaction [qRT-PCR]; left) of *Bcat1* in thymocytes obtained from 6-8-week-old C57/Bl6 mice and leukemic cells from 6 Δ*E-NOTCH1* T-cell acute lymphoblastic leukemia (T-ALL) tumors (NOTCH1-T). Significance was calculated using an unpaired two-tailed *t* test. $^{**}P<0.01$. Western blot (right) showing protein expression levels of ICN1 and Bcat1. β-actin and tubulin are shown as loading controls. Graphical representation of Bcat1/β-actin ratios (extreme right). Bars represent mean values. ICN1: intracellular NOTCH1. (C) Box plot showing the expression of *BCAT1* mRNA in T-ALL patients (N=57) and thymocyte subsets (7 thymocyte and mature T-cell subsets derived from [N=3] independent donors; quantile-normalized microarray results downloaded from GSE33469 and GSE33470). $CD3^+$ and $CD3^-$ DP cells were grouped together. $CD1^+$ and $CD1^-CD34^+$ cells were grouped together. Boxes represent first and third quartiles and line represents the median. Statistical analysis between groups was performed using unpaired two-sided *t* test. (D) BCAT1 transcript (top) and protein levels (bottom) in total human thymus, *NOTCH1* wild-type and *NOTCH1*-activated/mutated patient derived T-ALL patient-derived xenografts (PDX). Significance was calculated using a non-parametric *t* test (Mann-Whitney). $^{**}P<0.01$. ICN1, MYC and PTEN protein levels are also shown. β-actin is shown as loading control. (E) PDX samples were treated *in vivo* with DBZ (10 μg/kg every 8 hours [h] for a total of 3 injections) or vehicle (dimethyl suldoxide [DMSO]) for 24 h before analysis of BCAT1 transcript levels. For statistical analysis, an unpaired *t* test was used. $^{**}P<0.01$, $^{***}P<0.001$. (F) *NOTCH1* chromatin immunoprecipitation (ChIP)-sequencing binding (left) in the *BCAT1* locus in HPB T-ALL cells. Inset shows the location of ChIP-quantitative polymerase chain reaction (qPCR) amplicons near NOTCH-1 peak region (P1-P2) and in a negative control region (NL). Chromatin from PF382 cells was subjected to ChIP using a NOTCH1 antibody (right). The indicated regions (P1, P2 and NL) were PCR amplified from the precipitated and input DNA. Fold enrichment was calculated as a ratio of amplification efficiency of ChIP sample over that of the immunoglobulin G (IgG) control. Shown are means ± standard deviation SD (N≥3). For statistical analysis, an unpaired *t* test was used. $^{***}P<0.001$. NS: not significant.

Canonical functions of BCAT1 in T-cell acute lymphoblastic leukemia

In order to examine the role of Bcat1 in T-ALL development, we used a NOTCH1-dependent T-ALL mouse model (Δ*E-NOTCH1*). Transduced bone marrow (BM) progenitor cells ($GFP^+Lineage^-cKit^+Sca1^+$) from *Bcat1* KO and *Bcat1* WT were transplanted into lethally irradiated C57BL/6J hosts (*Online Supplementary Figure S6A*). Despite no evidence of engraftment defects 3 weeks post-transplant, mice receiving *Bcat1* KO Δ*E-NOTCH1* GFP^+ cells showed a significant delay in succumbing to leukemia respect to mice receiving *Bcat1* WT Δ*E-NOTCH1* GFP^+ cells (Figure 2A). The immunophenotype of established leukemias was similar amongst genotypes (*Online Supplementary Figure S6B*). We thus hypothesized that Bcat1 may be implicated in cell cycle progression or apoptosis of T-ALL cells. To examine this, we evaluated Edu incorporation and Annexin V staining in leukemic cells obtained from diseased animals. *Bcat1* KO T-ALL cells showed a decrease in the proportion of cells in the S-phase of the cell cycle (Figure 2B) and a modest increase in apoptotic cells (*Online Supplementary Figure S6C*). These results suggest that Bcat1 promotes survival and proliferation of *NOTCH1*-mutant T-ALL. We thus examined the *in vitro* and *in vivo* effects of *BCAT1* gene depletion by short-hairpin RNA (shRNA) in human leukemia cell lines expressing high levels of the protein. *Bcat1* silencing was associated with cell cycle arrest at the G1 phase (Figure 2C; *Online Supplementary Figure S7A*), inhibition of proliferation (Figure 2D), and induction of apoptosis (*Online Supplementary Figure S7B*) *in vitro* and decreased tumor growth *in vivo* (Figure 2E, F; *Online Supplementary Figure S7C*). Different cell lines exhibited differential sensitivity to the effects of BCAT1 depletion, which was also dependent on the type of assay used. Whereas BCAT1-silenced MOLT4 cells were far more apoptotic than CCRF-CEM cells *in vitro* (*Online Supplementary Figure S7B*), the opposite was true for tumor growth *in vivo*. Indeed, BCAT1 silencing in CCRF-CEM cells strongly affected their growth *in vivo* (Figure 2E), whereas, in MOLT4 cells, it yielded only a modest reduction in tumor burden and a moderate increase in survival (Figure 2F; *Online Supplementary Figure S7C*). BCAT1-silenced DND41 cells also recorded a high degree of apoptosis (*Online Supplementary Figure S7B*). We speculate that loss of BCAT1 in human T-ALL is associated with cell cycle arrest, apoptosis, and delayed tumor growth *in vivo*. In order to determine the putative mechanism behind the functional dependence of *NOTCH1*-mutant T-ALL cells on Bcat1, gene expression analysis was performed by RNA sequencing on leukemic cells isolated from spleens of diseased mice at the moment of sacrifice. Comparison of gene expression profiles of *Bcat1* WT and *Bcat1* KO Δ*E-NOTCH1* tumors identified 470 differentially expressed genes (≥2 fold change, $P<0.05$, false discovery rate [FDR] ≤0.1; Figure 3A; *Online Supplementary Table S2*). The majority of these genes showed decreased expression in *Bcat1* KO Δ*E-NOTCH1* tumors (*data not shown*). Gene set enrichment analysis (GSEA) identified four significantly different pathways: “G2M checkpoint”, “mitotic spindle”, “epithelial mesenchymal transition”, and “E2F targets”, all downregulated in *Bcat1* KO Δ*E-NOTCH1* cells (*Online Supplementary Table S3*; Figure 3B). On the other hand, GSEA analysis identified 18 significantly different pathways upregulated in *Bcat1* KO Δ*E-NOTCH1* cells, including “DNA repair”, “apoptosis”, and “p53 pathway” (*Online Supplementary Table S3*; Figure 3C). These results are consistent with our functional data and suggest that Bcat1 may be implicated in regulating the DNA damage response (DDR). To follow-up on this possibility, we evaluated the levels of γH2AX, a surrogate marker of DNA damage and double strand breaks (DSB) abundance in Bcat1-depleted cells. We found that *Bcat1* KO or BCAT1-de-

pleted cells had higher basal levels of γH2AX compared to Bcat1-expressing cells (Figure 3D).

Subsequently, we examined the metabolic impact of Bcat1 depletion on Δ*E-NOTCH1* leukemias. Briefly, we extracted metabolites from *Bcat1* WT and *Bcat1* KO Δ*E-NOTCH1* tumors, and quantified 56 metabolites by mass spectrometry to examine the metabolic impact of *Bcat1* loss on Δ*E-NOTCH1* leukemias (Figure 3E). We found N=19 differentially expressed metabolites between the pairs of compared *Bcat1* WT and *Bcat1* KO Δ*E-NOTCH1* tumors (Figure 3E). Of these, four metabolites (leucine, glutamine, 3-hydroxy-butyrate [3-HB] and lactic acid) were consistently modulated in other compared tumors (*data not shown*). Further, we performed $^{13}C_6$-Leucine stable-isotope tracing experiments to track the metabolic fate of BCAA in Δ*E-NOTCH1* leukemias. The results, which are shown in *Online Supplementary Figure S8*, indicated that $^{13}C_6$-Leucine was readily taken up by *Bcat1* WT tumors and that *Bcat1* KO tumors had increased levels of (m+6) leucine compared to WT tumors, presumably due to lack of Bcat1. Again, a relevant amount of labeled leucine was incorporated in 3-HB in both groups, with *Bcat1* KO tumors showing increased levels of (m+2 and m+3) 3-HB compared to WT tumors (*Online Supplementary Figure S8*). On the other hand, major TCA metabolites (with the exception of citrate) exhibited very low isotopic labeling indicating that Δ*E-NOTCH1* leukemias probably do not utilize BCAA for the replenishment of the TCA cycle. This result may however be influenced by our experimental approach using $^{13}C_6$-Leucine bolus injection rather than constant infusion.

The BCAT1 inhibitor, ERG245, recapitulates the functional consequences of Bcat1 depletion

Given our observations that BCAT1 could be a therapeutic target in T-ALL, we evaluated the effects of a novel BCAT1-specific inhibitor, ERG245.[25] Treatment of Δ*E-NOTCH1 Bcat1* WT leukemias with ERG245 was highly apoptotic and induced a potent cell cycle arrest (Figure 4A, B; *Online Supplementary Figure S9A, B*). Interestingly, Δ*E-NOTCH1 Bcat1* KO leukemias were almost refractory to this drug, even at high concentrations (Figure 4C). On the other hand, human T-ALL cell lines and PDX samples were less sensitive to the effects of ERG245, with only high doses determining effects on viability or cell cycle (Figure 4D, E; *Online Supplementary Figures S9C, D* and *S10A, B*). We further performed $^{13}C_6$-Leucine stable-isotope tracing experiments to examine the metabolic impact of BCAT1 inhibition on Δ*E-NOTCH1* leukemias. Briefly, NOTCH1-T-tumor bearing mice were treated *in vivo* with vehicle control or ERG245,[25] and perfused with $^{13}C_6$-Leucine just prior sacrifice. Cellular metabolites from snap-frozen spleens were then extracted and quantified. The results, which are shown in *Online Supplementary Figure S11*, indicated that $^{13}C_6$-Leucine was readily uptaken by the tumors and that tumors treated with ERG245 had increased levels of (m+6) leucine compared to tumors treated with vehicle-control, presumably due

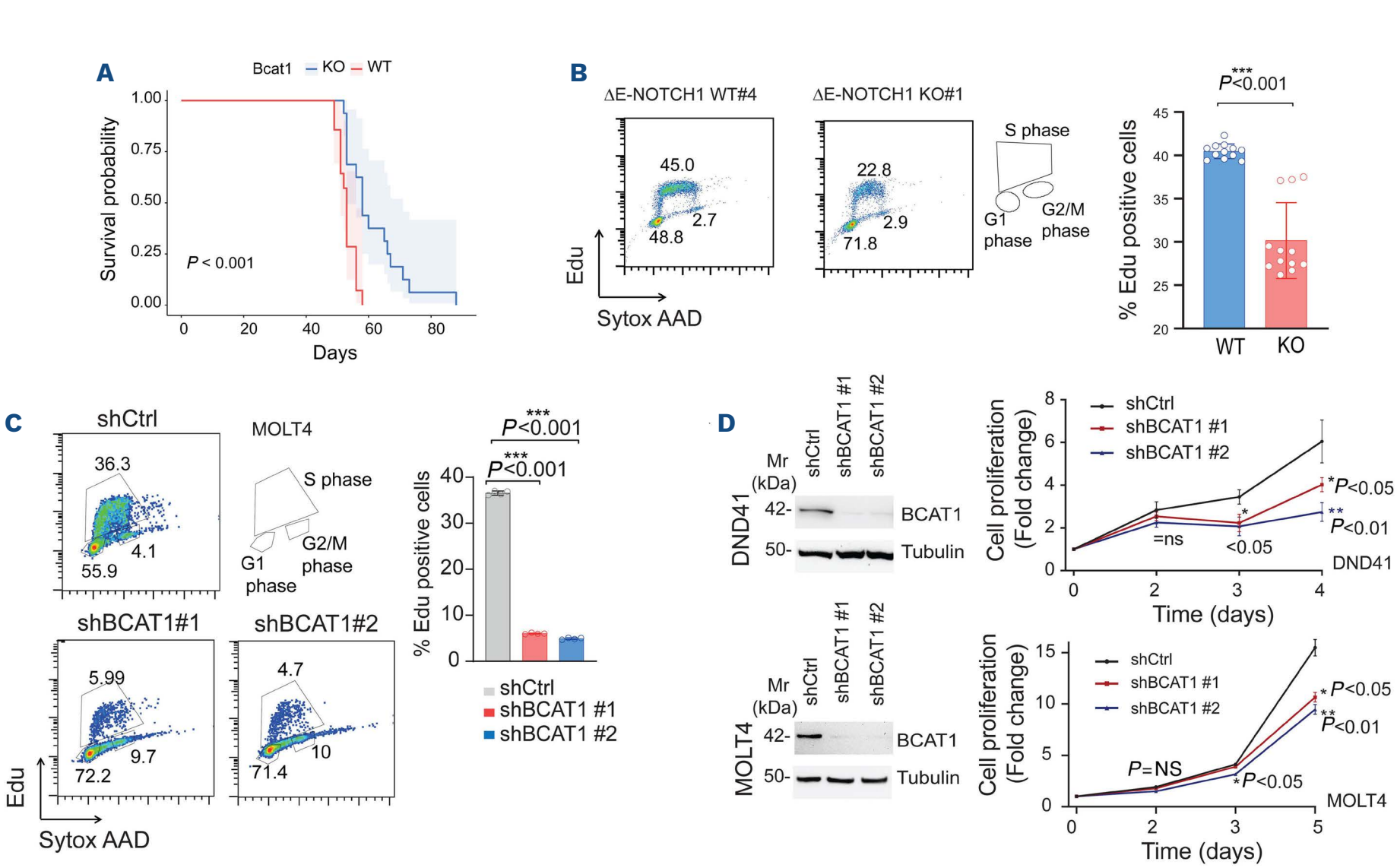

Continued on following page.

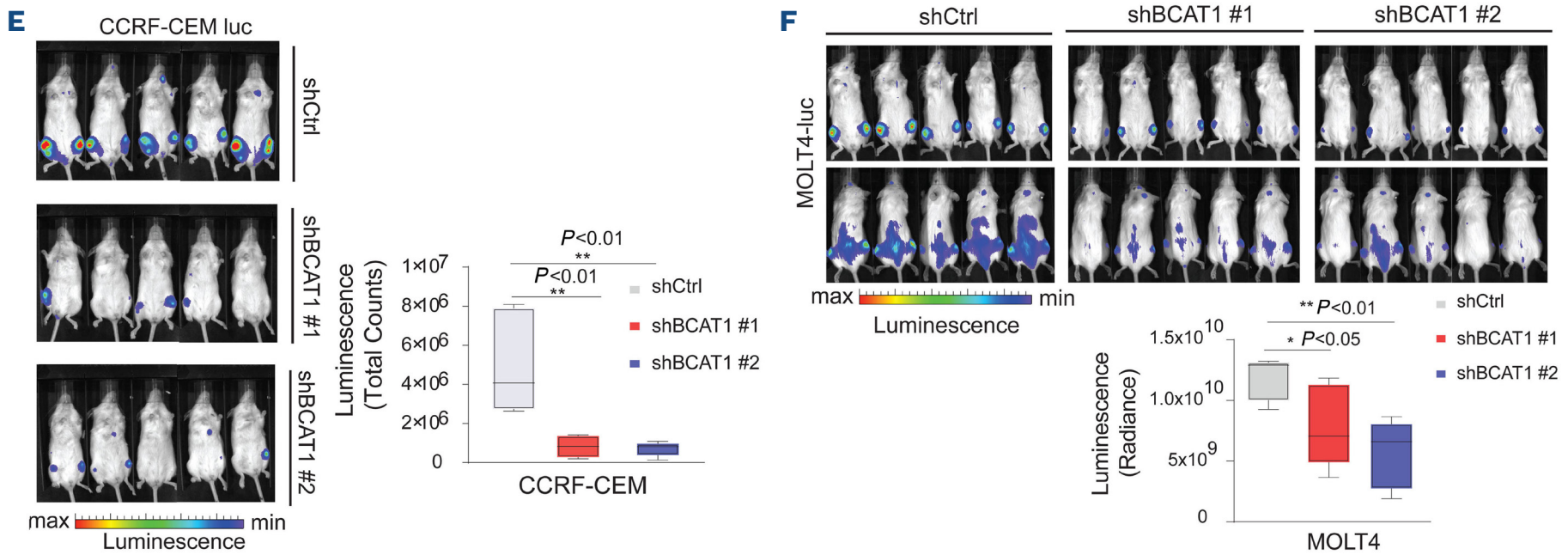

Figure 2. Functional effects of BCAT1 depletion. (A) Kaplan-Meier survival curves of overall survival in lethally irradiated C57BL/6J hosts transplanted with bone marrow (BM) cells (wild-type [WT] or knockout [KO] for *Bcat1*) transduced with Δ*E-NOTCH1* allele. Data from 2 independent transplantation experiments were pooled together. Log-rank Mantel-Cox test was performed to calculate *P* value. ***$P<0.001$. Shaded area represents 95% confidence interval (CI). (B) Representative plots (left) and bar graph representation (S-phase fraction; right) of *ex vivo* EdU incorporation in Δ*E-NOTCH1* leukemias WT and null for *Bcat1*. Data for bar graph is shown as mean ± standard deviation (SD). Significance was calculated using an unpaired two-tailed *t* test. ***$P<0.001$. (C) Representative plots (left) and bar graph representation (S-phase fraction; right) of MOLT4 cells transduced with small hairpin control vector (shCTRL), shBCAT1 #1 or shBCAT1 #2 7 days post-puromycin selection and assessed for EdU incorporation by fluorescence-activated cell sorting (FACS) analysis. Data for bar graph is shown as mean ± standard deviation (SD). Significance was calculated using an unpaired two-tailed *t* test. ***$P<0.001$. (D) T-ALL cells were transduced with control vector (shCTRL) or vector containing shRNA sequences against *BCAT1* (shBCAT1 #1, shBCAT1 #2). Expression of BCAT1 and tubulin was analyzed by immunoblotting 7 days post transduction (left panels) in DND41 and MOLT4. Starting from 7 days post-puromycin selection, cell proliferation was evaluated by determining cell number (DND41) or ATP levels by bioluminescence (MOLT4). Significance was calculated using an unpaired two-tailed *t* test. *$P<0.05$, **$P<0.01$. (E) Representative images of bioluminescence (left) and quantitative analysis of tumor burden (right) in NSG mice xenografted with CCRF-CEM cells expressing luciferase and transduced with shCTRL or shBCAT1 (#1 and #2). Analysis after 15 days post-transplant is shown. Significance was calculated using an unpaired two-tailed *t* test. **$P<0.01$. (F) Representative images of bioluminescence (top) and quantitative analysis of tumor burden (bottom) in NSG mice xenografted with MOLT4 cells expressing luciferase and transduced with shCTRL or shBCAT1 (#1 and #2). Analysis after 15 days post-transplant is shown. Significance was calculated using an unpaired two-tailed *t* test. *$P<0.05$, **$P<0.01$.

to inhibition of Bcat1 (*Online Supplementary Figure S11*). Two major metabolic events were observed with BCAT1 inhibition: i) a partial break in the TCA cycle between citrate and succinate, and ii) increased synthesis of 3-HB. In *Online Supplementary Figure S11*, accumulation of citrate and isocitrate are noted with a concomitant decrease in the levels of succinate and fumarate. A similar TCA cycle break was reported by Ko *et al.* in LPS-stimulated macrophages treated with a different but structurally related BCAT1 inhibitor.[26] Considering that the accumulation of TCA components previously noted in NOTCH1-T tumors (*Online Supplementary Figure S1D*), the break in the TCA cycle with BCAT1 inhibition constitutes a significant metabolic shift. Again, with the exception of citrate, major TCA metabolites exhibited limited isotopic labeling indicating that NOTCH1-T tumors may not utilize BCAA for the replenishment of the TCA cycle, at least under our experimental conditions of bolus injection. ERG245- driven inhibition of BCAT1 induced a modest decrease in the levels of isoleucine and valine (*data not shown*) in tandem with an increase in the isotopic labeling of citrate and 3-HB. Acetyl-CoA or succinyl-CoA (and propionyl-CoA) are the main end-products of BCAA metabolism, with acetyl-CoA that can be used to synthesize citrate and/or ketone bodies such as acetoacetate and 3-HB. These findings are similar to the metabolic effects obtained in *Bcat1* KO Δ*E-NOTCH1* tumors (*Online Supplementary Figure S8*). We speculate that, following BCAT1 inhibition or depletion, there is a shift towards leucine and 3-HB synthesis. 3-HB is known to act as an energy source in the absence of sufficient glucose and to inhibit class I histone deacetylases (HDAC),[27] thus influencing the acetylation state of proteins and/or the epigenetic regulation of genes.

BCAT1 depletion increases chemosensitivity of T-cell acute lymphoblastic leukemia cells and is dependent on its enzymatic activity

Given that our results implicate BCAT1 in regulating DDR, we examined if the cytotoxicity of DSB-inducing agents increases in the absence of BCAT1. The data suggest that BCAT1-depletion significantly enhances the sensitivity of murine and human T-ALL cells to etoposide (Figure 5A-C; *Online Supplementary Figure S10C, D*). Δ*E-NOTCH1 Bcat1* KO leukemias were particularly sensitive to etoposide (Figure

5A). In Figure 5B, early apoptotic CCRF-CEM cells (Annexin$^+$ Sytox Red$^-$) and late apoptotic or necrotic CCRF-CEM cells (Annexin$^+$ Sytox Red$^+$) were evident at 48 h of etoposide treatment; both populations increased significantly when etoposide was combined with BCAT1 depletion (Figure 5B). Similar results were obtained with DND41 (*Online Supplementary Figure S10C*) and MOLT4 cells (*Online Supplementary Figure S10D*). Increased chemosensitivity in BCAT1-depleted cells was also observed when cells were exposed to other drugs such as doxorubicin (*Online Supplementary Figure S10E, F*). To understand the effect of BCAT1 silencing on etoposide-induced DNA damage, we examined the presence of DNA DSB in CCRF-CEM cells transduced with *shBCAT1* after treatment with etoposide for different time periods by determining the levels of γH2AX, a surrogate marker of DSB abundance (Figure 5C; *Online Supplementary Figure S12A*). Additionally, we performed a neutral comet assay to determine the extent of DNA damage (DSB). In this

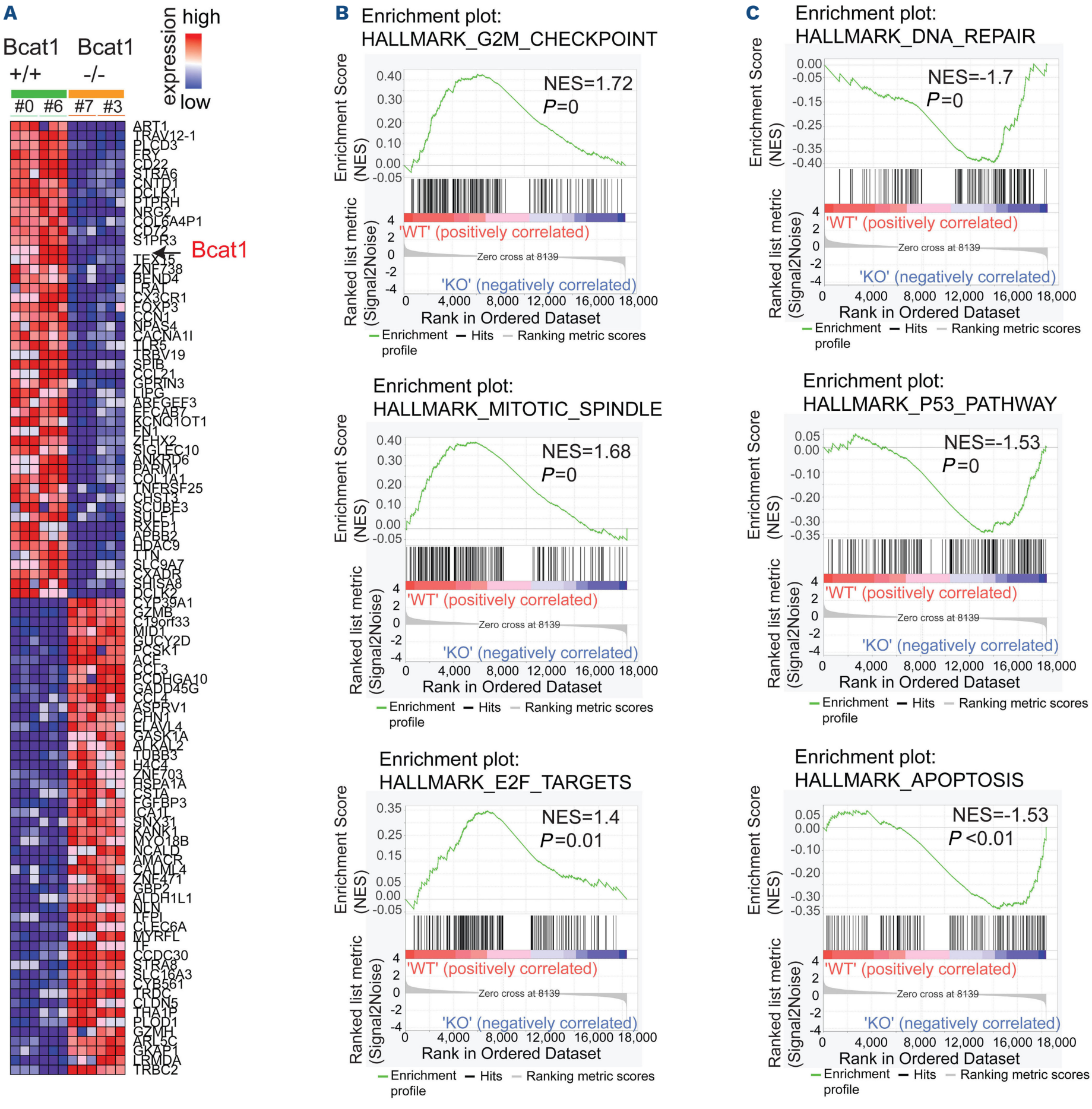

Continued on following page.

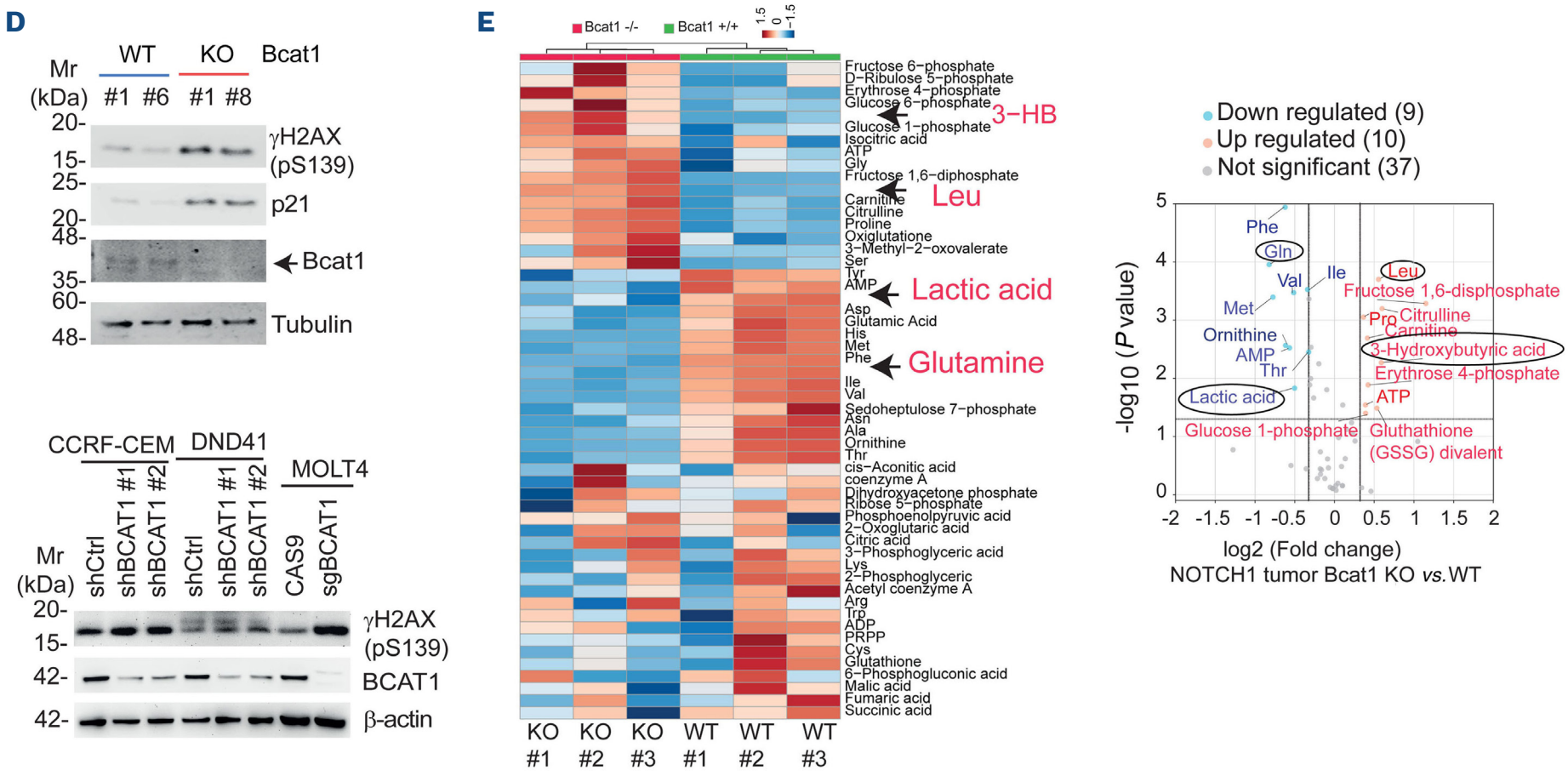

Figure 3. Canonical functions of Bcat1. (A) Heat map representation of the top down-and upregulated genes between Δ*E-NOTCH1* tumors wild-type (WT) or knockout (KO) for *Bcat1*. Two independent WT and KO tumors were analyzed. *Bcat1* gene is highlighted in red. (B) Gene set enrichment analysis (GSEA) identified 3 significantly enriched gene sets involved in cell cycle regulation downregulated in *Bcat1* KO T-cell acute lymphoblastic leukemia (T-ALL) cells. The normalized enrichment score (NES) and the nominal *P* value are illustrated. (C) GSEA identified 3 significantly enriched gene sets involved in DNA damage response upregulated in *Bcat1* KO T-ALL cells. The NES and the nominal *P* value are illustrated. (D) Immunoblots of γH2AX, p21 and Bcat1 in tumors WT or KO for *Bcat1* (top). α-tubulin is shown as loading control. T-ALL cells (CCRF-CEM, DND41, MOLT4) transduced with shCTRL/CAS9 or shBCAT1 (#1 and #2)/sgBCAT1 were analyzed by immunoblotting for γH2AX and BCAT1 (bottom). β-actin is shown as loading control. (E) Heatmap representation (left) of the top 50 differentially expressed metabolites identified by capillary electrophoresis time-of-flight mass spectrometry (CE-TOFMS) between Δ*E-NOTCH1* leukemias WT and KO for *Bcat1*. Metabolites that are significantly and consistently differentially expressed in multiple comparisons are highlighted in red. Volcano plot (right) showing differentially expressed metabolites (≥1.5 fold change, $P<0.05$; in red and blue) identified by CE-TOFMS between Δ*E-NOTCH1* leukemias WT and KO for *Bcat1*. Metabolites that are significantly and consistently differentially expressed in multiple comparisons are encircled.

assay, the percent tail DNA can be used to quantitate DNA damage. We found that BCAT1-depleted cells exposed to etoposide presented considerably more tail DNA compared to control cells, especially at the 6 h time point (Figure 5D). We also examined the phosphorylation status of key proteins that control activation of different DNA DSB repair pathways (DNA-PK for c-NHEJ pathway and ATM for HR pathway) or cell cycle arrest (CHK2 and p53). *Online Supplementary Figure S12B* indicates that both c-NHEJ and HR pathways were involved in repairing etoposide-induced DNA damage. Whereas control and BCAT1-depleted CCRF-CEM cells exhibited similar rates of ATM phosphorylation, DNA-PK was subject to an accentuated phosphorylation in BCAT1-depleted cells (*Online Supplementary Figure S12B*). Interestingly, increased DNA sensing was not associated with DNA DSB repair but with further DNA damage, as intimated by the dramatic increase in the levels of γH2AX in BCAT1-depleted cells compared to control cells (Figure 5C; *Online Supplementary Figure S12A, B*). The combination of *BCAT1* silencing and etoposide treatment was also associated with increased levels of phosphorylated CHK2 and p53 (*Online Supplementary Figure S12B*). Cleaved PARP-1 was observed only at 24 h of etoposide treatment suggesting that the failure of the cells with depleted BCAT1 to repair DNA DSB leads to extensive DNA damage and eventually apoptosis (*Online Supplementary Figure S12A*).

We next determined whether the metabolic function of BCAT1 contributes in modulating the sensitivity to DNA damaging agents. To this end we constructed a BCAT1 catalytic-inactive mutant where we abolished transaminase activity through mutation of lysine 222 to alanine (*BCAT1* ^{K222A})[28]. Next, we analyzed the phenotypic impact of expressing wild-type *BCAT1* (*BCAT1*^{WT}) and *BCAT1* ^{K222A} in BCAT1-depleted CCRF-CEM cells treated with etoposide. We found that overexpression of *BCAT1*^{WT} was able to partially rescue the phenotype of BCAT1-depleted cells (*Online Supplementary Figures S13A, S12C*), while *BCAT1* ^{K222A}-overexpressing cells maintain sensitivity to etoposide much like parental BCAT1-depleted cells (*Online Supplementary Figure S13A*, *C*). These data suggest that BCAT1 catalytic

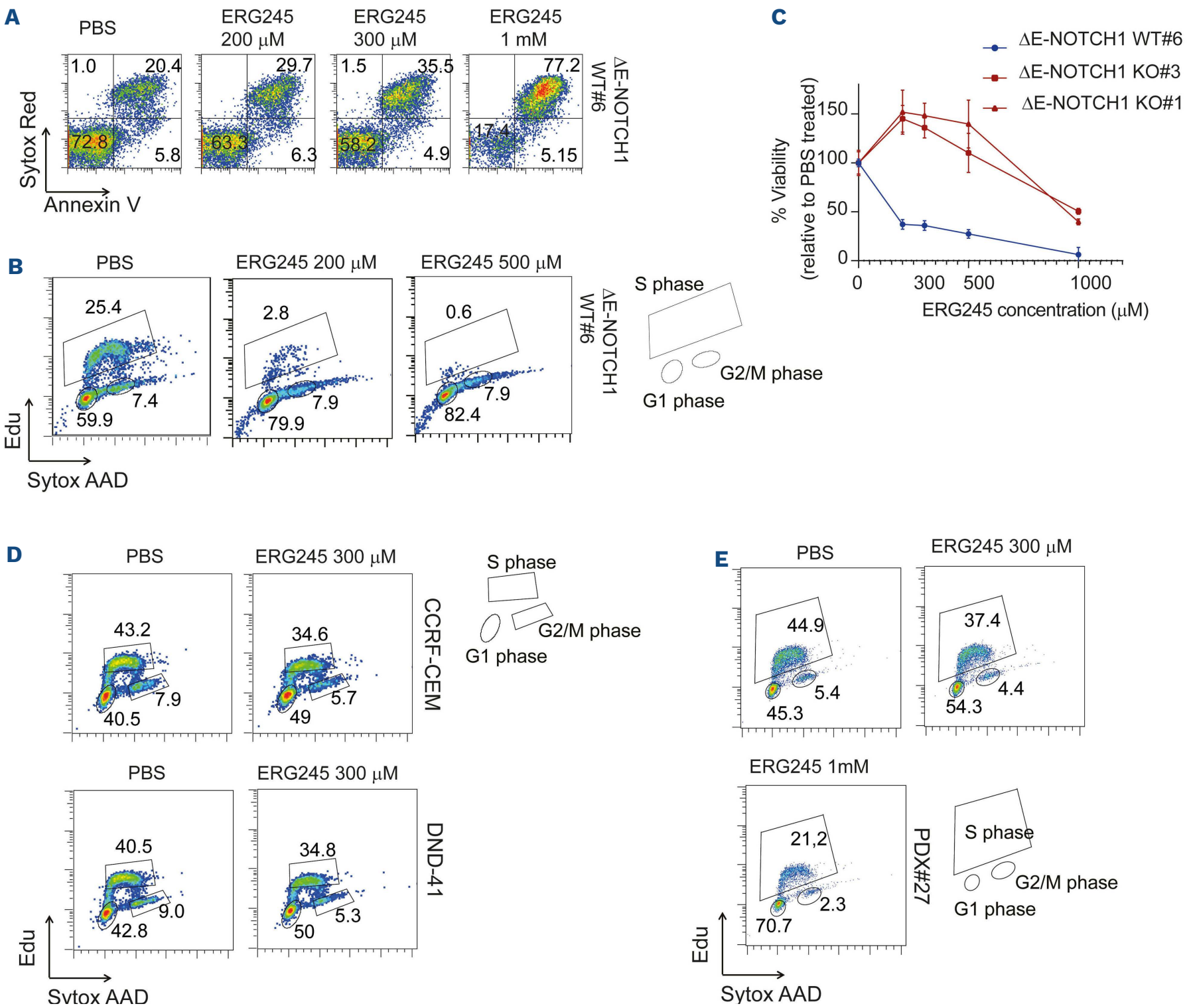

Figure 4. ERG245, a BCAT1-specific inhibitor mimics the functional consequences of Bcat1 depletion. (A) Representative plots of apoptosis in Δ*E-NOTCH1* leukemia wild-type for *Bcat1* (WT#6) treated *in vitro* for 48 hours (h) with phosphate-buffered saline (PBS) (vehicle) or increasing doses of ERG245 (200 μM - 1 mM). (B) Representative plots of *ΔE NOTCH1* leukemia WT for *Bcat1* (WT#6) treated *in vitro* for 48 h with PBS (vehicle) or increasing doses of ERG245 (200-500 μM). Cells were then assessed for EdU incorporation by fluorescence-activated cell sorting (FACS) analysis. (C) Representative cell viability analysis in Δ*E-NOTCH1* tumors WT (WT#3) or knockout (KO) (KO#3, #1) for *Bcat1*. Murine T-cell acute lymphoblastic leukemia (T-ALL) cells were treated *in vitro* for 48 h with PBS (vehicle) or increasing doses of ERG245 (100 μM - 1 mM). Data is shown as mean ± standard deviation (SD). (D) Representative plots of T-ALL cell lines (CCRF-CEM, DND41) treated *in vitro* for 72 h with PBS (vehicle) or ERG245 (300 μM). Cells were then assessed for EdU incorporation by FACS analysis. (E) Representative plots of PDX#27 treated *in vitro* for 72 h with PBS (vehicle) or increasing doses of ERG245 (300 μM - 1 mM). Cells were then assessed for EdU incorporation by FACS analysis.

activity is required for maintaining resistance to DNA damaging agents such as etoposide. Since we found 3-HB (a putative HDAC inhibitor) to accumulate in *Bcat1* KO and ERG245-treated murine T-ALL, we evaluated whether this metabolite could be implicated in modulating sensitivity to etoposide. CCRF-CEM cells treated with increasing doses of 3-HB showed sensitization to the cytotoxic effects of etoposide (*Online Supplementary Figure S13B*). Similar results were obtained in a human T-ALL PDX model (PDX#47; *Online Supplementary Figure S12D-F*). Interestingly, the well-known HDAC inhibitor, NaB, was also highly effective in sensitizing cells to the cytotoxic effects of etoposide (*Online Supplementary Figures S13B* and *S12D-F*), further suggesting a common mode of action between 3-HB and NaB. Following up on these observations, we initially determined whether Bcat1/BCAT1 depletion or inhibition could modulate the epigenetic state (acetylation) of histones. We found H3K27 acetylation to be consistently increased in

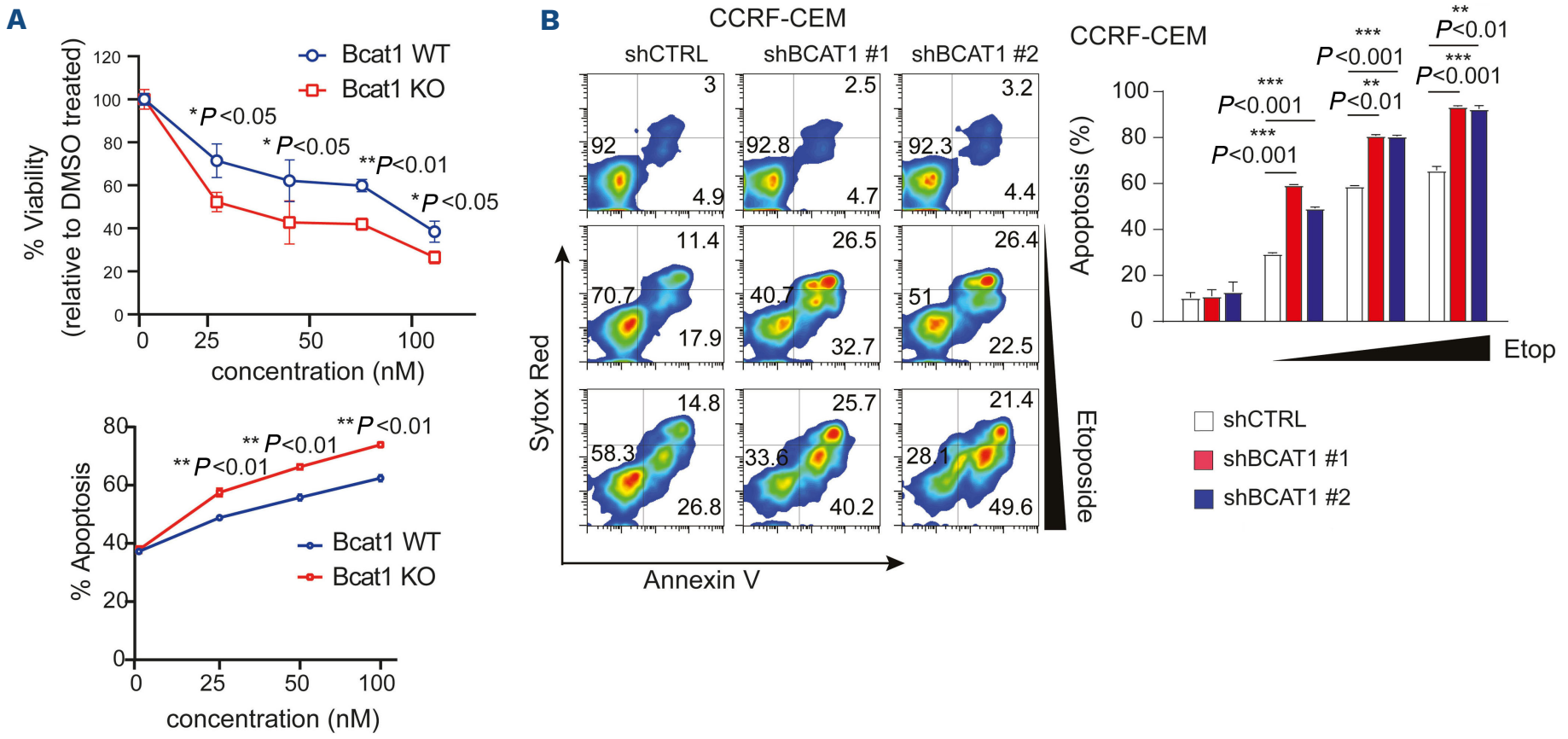

Figure 5. BCAT1 loss induces a dysfunctional DNA damage response following etoposide treatment. (A) Representative cell viability analysis (top) in Δ*E-NOTCH1* tumors wild-type (WT) (WT#1) or knockout (KO) (KO#6) for *Bcat1*. Murine T-cell acute lymphoblastic leukemia (T-ALL) cells were treated *in vitro* for 48 hours (h) with dimethyl sulfoxide (DMSO) (vehicle) or increasing concentrations of etoposide (25-100 nM). Data is shown as mean ± standard deviation (SD). Significance was calculated using an unpaired two-tailed *t* test. $^{*}P<0.05$, $^{**}P<0.01$. Quantification of apoptosis (bottom) in Δ*E-NOTCH1* tumors WT (WT#1) or KO (KO#6) for Bcat1 treated *in vitro* for 48 h with DMSO (vehicle) or increasing concentrations of etoposide (25-100 nM). Data is shown as mean ± SD. Significance was calculated using an unpaired two-tailed *t* test. $^{*}P<0.05$, $^{**}P<0.01$. (B) Representative plots of apoptosis (left) in CCRF-CEM T-ALL cells transduced with small hairpin control vector (shCTRL) or shBCAT1 (#1 and #2) and treated *in vitro* for 48 h with DMSO (vehicle) or etoposide (100 nM or 1 μM). Quantification of apoptosis (right) in CCRF-CEM T-ALL cells transduced with shCTRL or shBCAT1 (#1 and #2) and treated *in vitro* for 48 h with DMSO (vehicle) or etoposide (100 nM - 2 μM). Significance was calculated using an unpaired two-tailed *t* test. $^{**}P< 0.01$, $^{***}P<0.001$. (C) Expression of cleaved PARP-1 and phosphorylated γH2AX was analyzed by immunoblotting in CCRF-CEM T-ALL cells transduced with shCTRL or shBCAT1 (#1 and #2) and treated *in vitro* for 48 h with DMSO (vehicle) or etoposide (1 μM). β-actin and GADPH are shown as loading controls. (D) Representative neutral comet images (left) performed in CCRF-CEM cells infected with a control shRNA (shCTRL) or BCAT1-targeting shRNA (shBCAT1#1, shBCAT1#2) either untreated or after etoposide treatment (1μM) for 2 or 6 hours. Dot plot (right) showing individual percentages of comet tail DNA. The median value of 50-80 nuclei per experimental condition is indicated. Statistical analysis was conducted by using the Mann-Whitney test. Data are representative of 2 independent experiments.

Bcat1 KO and BCAT1-depleted cells (*Online Supplementary Figure S12G, H*), similarly to 3-HB treated cells (*Online Supplementary Figure S12I*). Interestingly, increased acetylation of proteins implicated in DDR response (p53, Ku70, Ku80)

was also found in BCAT1-depleted cells, especially after etoposide treatment (*Online Supplementary Figure S12J*). These results suggest that altered acetylation of signaling proteins may contribute to the chemo-sensitizing effect of BCAT1 depletion/inhibition.

BCAT1 overexpression correlates with poor survival and its pharmacological inhibition synergizes with DNA-damaging chemotherapy in T-cell acute lymphoblastic leukemia cell

In order to investigate the putative clinical relevance of high BCAT1 expression, we used the TARGET T-ALL cohort composed of over 260 T-ALL patients.[16] Using the mean BCAT1 expression level as the cutoff for subdividing high and low BCAT1 expression, we found that BCAT1 levels had a prognostic significance (*Online Supplementary Figure S14A*). Another disease characterized by frequent constitutive activation of the NOTCH1 signaling cascade (by mutational and non-mutational mechanisms) is chronic lymphocytic leukemia (CLL).[29,30] We also evaluated the prognostic significance in a profiled CLL cohort (N=107) with known clinical response (survival).[31] Using the mean BCAT1 expression level as the cutoff for subdividing high and low BCAT1 expression, BCAT1 levels were also found to have a prognostic significance (*Online Supplementary Figure S14A*). These results suggest that BCAT1 may have a prognostic significance in these two NOTCH1-dependent leukemias and may further represent a valid therapeutic target.

Following-up on our observation that knock-down of BCAT1 increased the sensitivity of T-ALL cells to DNA damaging agents, we investigated whether pharmacological inhibition of BCAT1 using ERG245 could also improve the antitumor efficacy of DNA damaging agents. We found that ERG245 potentiated the effects of DNA-damaging drugs such as etoposide (Figure 6A, B; *Online Supplementary Figures S14B, C* and *S15A-C*), cytarabine (*Online Supplementary Figure S15C*) and doxorubicin (*Online Supplementary Figure S15C*) in T-ALL cell lines (MOLT4, CCRF-CEM, and DND41) and PDX cells (Figure 6C, D; *Online Supplementary Figures S14D-J*, *S15D, E* and *S16A-C*). The combinatory effect of ERG245 and a DNA-damaging agent was synergistic in most cases and most pronounced for etoposide (*Online Supplementary Figure S15C*). Levels of γH2AX increased dramatically following addition of ERG245 to T-ALL cells treated with etoposide (Figure 6B; *Online Supplementary Figures S14F, S16A*). That increase was accompanied by induction of apoptosis as indicated by the presence of cleaved PARP-1. Next, we used a xenograft-based approach to test the effects of combining BCAT1 inhibition with etoposide in *in vivo* models of T-ALL. We injected luciferase-expressing PDX#27 (PDX#27-luc) cells into NSG mice and treated them with vehicle, ERG245 (30 mg/kg, 3 times a week), etoposide (15 mg/kg, twice a week) or the combination of the two drugs for 14 days. Tumor burden was evaluated using bioluminescence, hCD45$^+$ staining, and spleen weight as human T-ALL is characterized by elevated levels of CD45$^+$ blasts and splenomegaly. Whereas etoposide treatment decreased tumor burden by almost one-log unit of bioluminescence compared to vehicle, the combination of etoposide and ERG245 decreased it by almost two-log units (Figure 6D). The efficacy of the combination treatment was additionally reflected in the other markers used to assess tumor growth: mice treated with etoposide and ERG245 exhibited lower levels of human CD45$^+$ blasts in the peripheral blood (PB; *Online Supplementary Figure S16B*), spleen and bone marrow (*data not shown*). Further, these mice did not show splenomegaly (*Online Supplementary Figure S16C*). Actually, our results suggest that mice in the combination group experienced almost complete elimination of tumor cells (N=5; blasts <1%) in PB, and all mice had experienced partial remission (>90% reduction of blasts compared to vehicle treated mice at day 28) in target organs (bone marrow, spleen). In contrast, mice that received etoposide monotherapy exhibited much smaller tumor burden decreases, while almost complete elimination of tumor cells (blasts <1% in any compartment) were absent in that group. Impact on overall survival was not evaluated. Similar results were obtained in another highly aggressive PDX model, PDX#19. Here, luciferase expressing PDX#19 (PDX#19-luc) cells were injected into NSG mice and treated with vehicle, ERG245 (30 mg/kg, 3 times a week), etoposide (10 mg/kg, twice a week) or the combination for 10 days before evaluating tumor burden (*Online Supplementary Figure S14G-J*). The data again highlight that BCAT1 inhibition greatly potentiates the antitumor activity of etoposide *in vivo*.

Discussion

The present study elucidates the unique role that BCAT1 plays in T-ALL. BCAT1 is the cytosolic enzyme commonly responsible for the reversible transfer of an amino group from leucine, isoleucine, and valine to α-ketoglutarate (α-KG) to form glutamate and the corresponding α-ketoacid.[32] Here, we report that BCAT1 is a downstream target of mutated NOTCH1. Mutations that activate NOTCH1 signaling are found in more than 65% of all T-ALL cases and considered a hallmark of the disease. Our experiments revealed that Notch1 binds to *Bcat1* promoter and increases *Bcat1* gene transcription early in the process of leukemogenesis in experimental models of T-ALL, as well as in clinical samples of patients suffering from the disease. Such an increase confers metabolic and other advantages to the leukemic cells. Compared to thymic tissues, we show that NOTCH1-T tumors exhibit elevated levels of TCA cycle metabolites. For the same tumors, we report a break in the TCA cycle with BCAT1 inhibition and impaired metabolic activity as determined by the downregulation of many essential metabolites. At the same time, BCAT1 inhibition

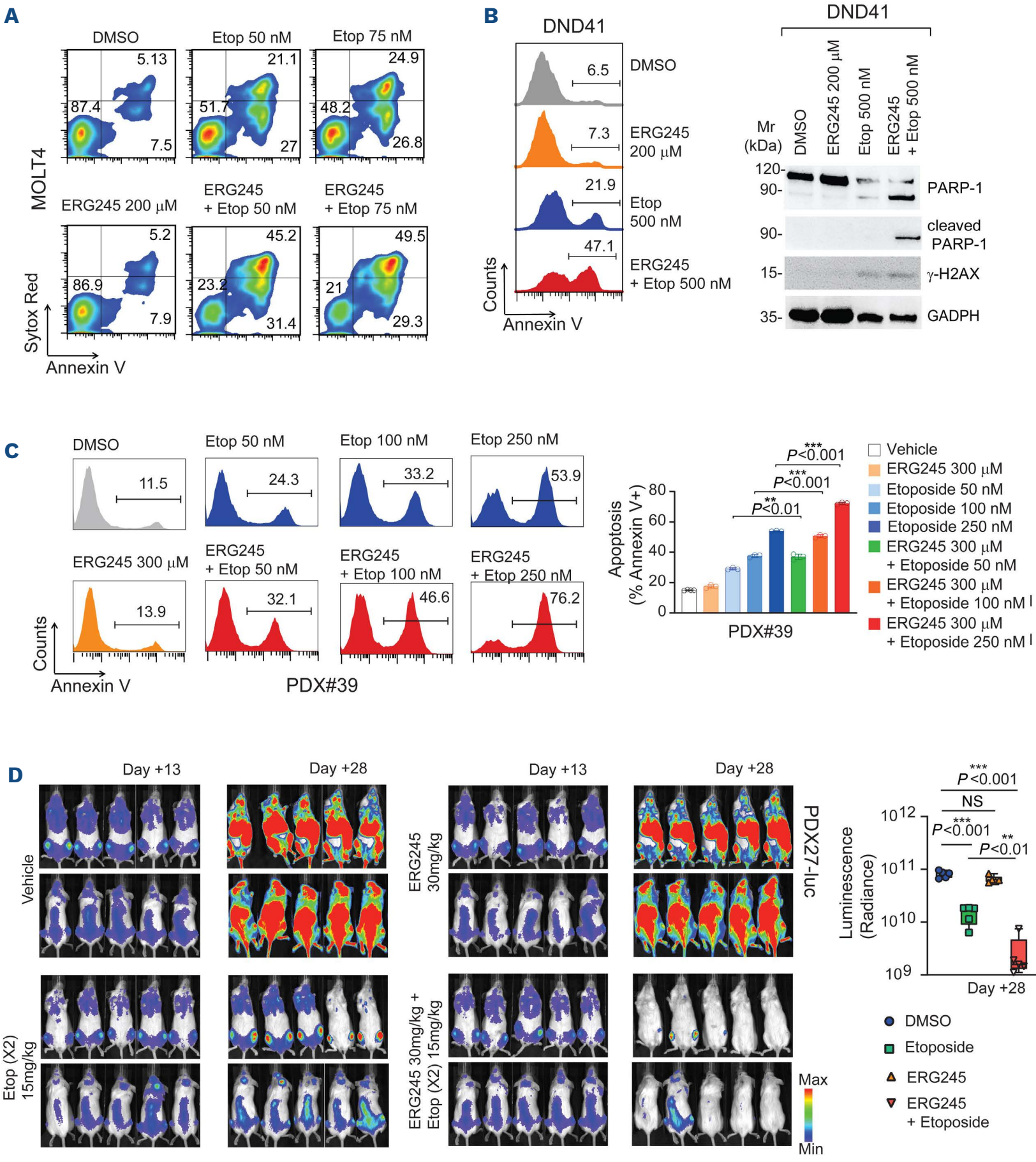

Figure 6. BCAT1-specific inhibition increases response to DNA-damaging agents, especially etoposide, *in vitro* and *in vivo*. (A) Representative plots of apoptosis in MOLT4 T-cell acute lymphoblastic leukemia (T-ALL) cells treated with vehicle (dimethyl sulfoxide [DMSO]), BCAT1 inhibitor (ERG245), etoposide (Etop; 50-75 nM) or the combination (ERG245 + Etop) for 48 hours (h). (B) Representative plots of Annexin V staining (left panels) in DND41 T-ALL cells treated with vehicle (DMSO), BCAT1 inhibitor (ERG245), Etop or the combination (ERG245 + Etop) for 48 h. Western blot analysis (right panels) of PARP-1 (total or cleaved PARP-1), and phosphorylated γH2AX in DND41 cells treated for 48 h with DMSO (vehicle), ERG245 (200 µM), Etop (500 nM) or ERG245 + Etop. GADPH was used as protein loading control. (C) Representative plots (left) and bar graph representation (right) of apoptosis (Annexin V-positive) in *ex vivo* obtained PDX#39 cells treated with vehicle (DMSO), BCAT1 inhibitor (ERG245), Etop (50-250 nM) or the combination (ERG245 + Etop) for 48 h. Significance was calculated using an unpaired two-tailed *t* test. $^{**}P<0.01$, $^{***}P<0.001$. (D) Representative images of bioluminescence (left) in NSG mice xenografted with PDX#27 cells expressing luciferase (PDX#27-luc) and treated with vehicle (DMSO), BCAT1 inhibitor (ERG245; 30 mg/kg 3 times a week), Etop (15 mg/kg twice a week) or the combination (ERG245 + Etop). Analysis before (day 13 post-transplantation) and 15 days after start of treatment (day 28 post-transplantation) is shown. Quantitative analysis of tumor load (right) via *in vivo* bioluminescence imaging of NSG mice xenografted with PDX#27-luc after treatment (day 28 post-transplantation) with vehicle (DMSO), BCAT1 inhibitor (ERG245), Etop or the combination (ERG245 + Etop). Significance was calculated using an unpaired two-tailed *t* test. $^{**}P<0.01$, $^{***}P<0.001$. NS: not significant.

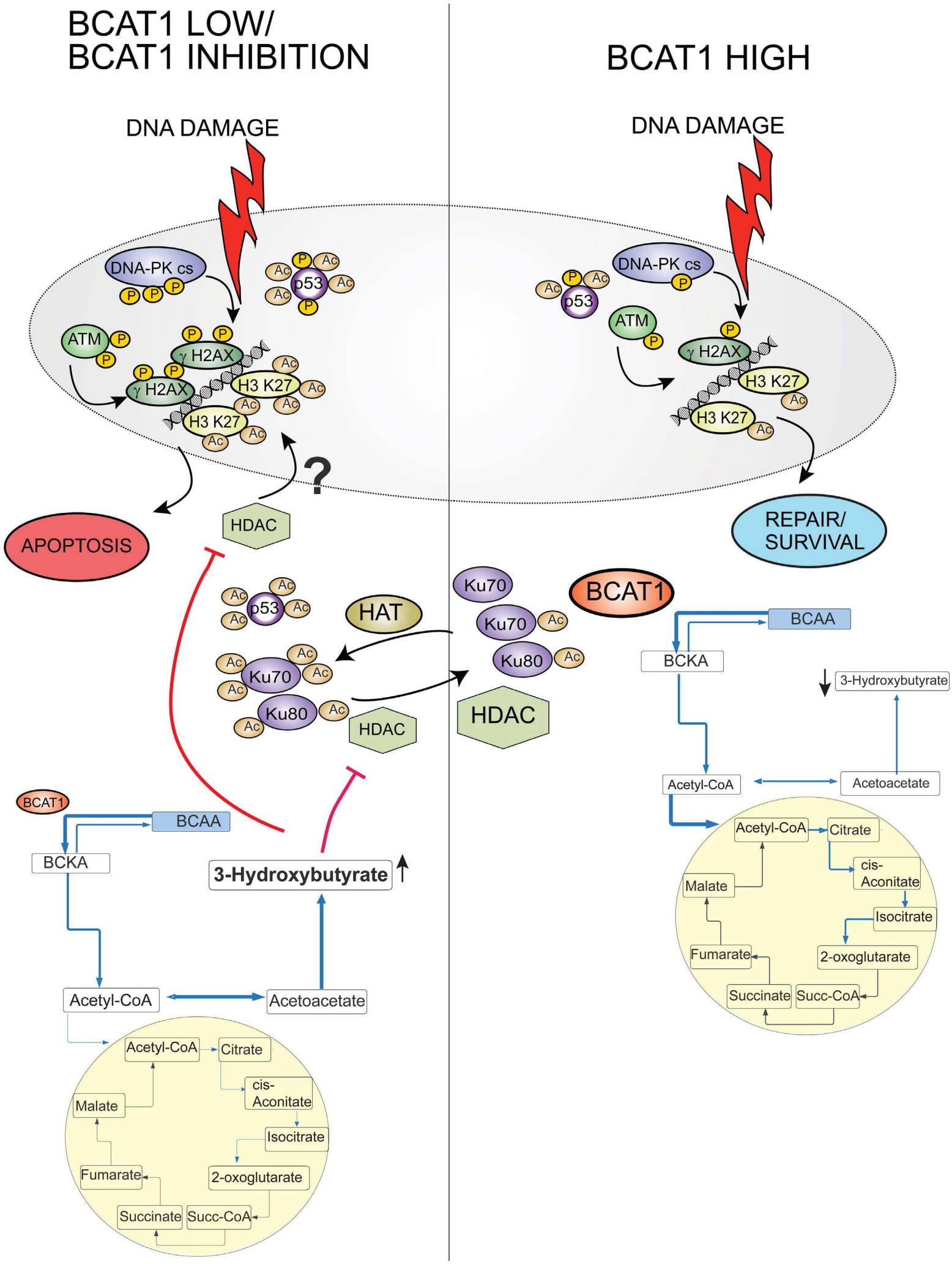

Figure 7. Schematic illustration of the proposed role of BCAT1 in regulating T-cell acute lymphoblastic leukemia response to DNA-damaging agents in BCAT1-high and BCAT1-silenced/functionally inhibited T-cell acute lymphoblastic leukemia cells. BCAT1 inhibition induces a partial break in the tricarboxylic acid cycle cycle between citrate and succinate leading to citrate accumulation and directing leucine metabolism towards 3-HB synthesis. 3-HB is known to act as an energy source in the absence of sufficient glucose and as it builds up it inhibits class I histone deacetylases (HDAC), leading to increased acetylation of proteins such as histones and DNA damage response proteins (including Ku70 and Ku80) modifying their activity[39,40] and possibly priming cells to the deleterious effects of DNA-damaging agents. Following the exposure to DNA-damaging agents (etoposide) this leads to accentuated DNA damage leading to cell death.

or Bcat1 depletion appears to redirect leucine metabolism towards synthesis of leucine and 3-HB, an HDAC inhibitor, suggesting that BCAT1 may also regulate protein acetylation. Indeed, we find increased acetylation of histones (H3K27) and repair proteins (Ku70/Ku80) in Bcat1/BCAT1-depleted cells. Another interesting finding was that BCAT1 depletion or inhibition resulted in increased levels of γH2AX, a marker of increased DNA damage. Although we do not provide any direct experimental evidence, this may be linked to an anti-oxidant role for the BCAT1 CXXC motif, normally buffering intracellular reactive oxygen species (ROS).[33]

Deletion of Bcat1 seems associated with faulty DDR and induction of apoptosis, especially following exposure to DNA-damaging agents. Collectively, our study indicates that NOTCH1 upregulates BCAT1 to metabolically reprogram the cells and to ensure cell survival upon DNA damage possibly through altered 3-HB synthesis and protein acetylation (see Figure 7). This is in line with numerous studies suggesting that NOTCH1 controls oncogenic pathways that promote cell proliferation and survival, metabolic reprogramming, and resistance to chemotherapy through transcriptional activation of downstream target genes. Although non-canonical functions have previously been assigned to BCAT1 and linked to its redox state,[25,28,34] increased sensitivity to etoposide in BCAT1-depleted cells seems to be dependent on its transaminase activity. We speculate that following BCAT1 depletion/inhibition, cells adapt increasing ketone body synthesis (3-HB) which initially has growth-promoting effects (through its anti-oxidant effect at low concentrations), but as it accumulates, it paradoxically promotes cell death through its capacity to inhibit HDAC[35,36] and promote protein acetylation. This accumulation of 3-HB seems to potentiate the cytotoxic effects of DNA-damaging agents such as etoposide. We hypothesize that NOTCH1 directly[9] and indirectly (through BCAT1 upregulation) represses DDR in order to promote cell survival in the presence of a genotoxic insult. The same mechanism might be at play during leukemogenesis, which allows for the accumulation of genetic lesions, the survival of the cells, and ultimately the onset of T-ALL.

The role of BCAT1 in leukemia and other cancers is currently an active area of research. Numerous reports have indicated that BCAT1 is a risk factor in multiple cancers: its expression is associated with tumor progression, increased chemoresistance, and poor prognosis.[37,38] In agreement, our experiments suggest that high BCAT1 expression correlates with poor survival in NOTCH1-driven malignancies (T-ALL, B-CLL) and that inhibition of BCAT1 increases the chemosensitivity of T-ALL cells towards cytotoxic drugs, known to induce DSB, such as the topoisomerase II inhibitor etoposide. In two aggressive PDX models, the combination of ERG245 and etoposide markedly reduced tumor burden, almost completely cleared CD45$^+$ blasts from the blood, and abolished splenomegaly in the majority of the treated animals indicating that BCAT1 could be a novel therapeutic target in T-ALL particularly in salvage protocols.

Disclosures

No conflicts of interest to disclose.

Contributions

LDM performed ChIP analyses, performed some in vitro experiments with inhibitors, performed qRT-PCR experiments and helped writing the first draft of the manuscript. VT generated NOTCH1-dependent mouse T-ALL, performed in vitro and in vivo therapeutic experiments and helped writing the first draft of the manuscript. AEP provided the BCAT inhibitor, helped designing in vivo therapeutic experiments and helped writing the manuscript. LDM and SDS helped setting up the protocol for performing the immunophenotypic characterization of the leukemia in Bcat1 WT and KO mice and performed some analyses. LM performed patient selection and provided clinical data. MP performed and helped interpreting IHC results. JL assisted in bioinformatical analyses. PVV assisted in analyzing ChIP-seq data and provided reagents. EP designed and performed some experiments, directed research, analyzed data and wrote the paper. All the authors read and edited the manuscript.

Acknowledgments

We thank Sonia Minuzzo for providing T-ALL xenografts and Laura Bonaldi for help with epifluorescence microscopy. We are grateful to Ilaria Talli for technical assistance in setting up methylation specific assays. Special thanks to Jiyang Yu and Angela Grassi for doing preliminary gene expression profiling analysis and help with bioinformatics analyses concerning the various datasets used in the present study. We are especially grateful to our co-author, Pieter van Vlierberghe, who recently passed away, for his enthusiastic contribution, warmth and friendship.

Funding

This work was supported by the Italian Foundation for Cancer Research (Fondazione AIRC) grants (to EP) (IG2018#22233); Ex 60% (to EP) (University of Padova).

Data-sharing statement

The study utilized, in part, publicly available datasets (Gene Expression Omnibus, Chinese Leukemia Genotype-Phenotype Archive). Raw data for this study were generated at HMT (Tokyo, Japan) and Active Motif (Waterloo, Belgium). Derived data supporting the findings of this study are available from the corresponding author upon reasonable request.

References

1. Terwilliger T, Abdul-Hay M. Acute lymphoblastic leukemia: a comprehensive review and 2017 update. Blood Cancer J. 2017;7(6):e577.
2. Pui CH, Robison LL, Look AT. Acute lymphoblastic leukaemia. Lancet. 2008;371(9617):1030-1043.
3. Belver L, Ferrando A. The genetics and mechanisms of T cell acute lymphoblastic leukaemia. Nature reviews Cancer. 2016;16(8):494-507.
4. Bongiovanni D, Saccomani V, Piovan E. Aberrant signaling pathways in T-cell acute lymphoblastic leukemia. Int J Mol Sci. 2017;18(9):1904.
5. Weng AP, Ferrando AA, Lee W, et al. Activating mutations of NOTCH1 in human T cell acute lymphoblastic leukemia. Science. 2004;306(5694):269-271.
6. Ferrando AA. The role of NOTCH1 signaling in T-ALL. Hematology Am Soc Hematol Educ Program. 2009;353-361.
7. Palomero T, Lim WK, Odom DT, et al. NOTCH1 directly regulates c-MYC and activates a feed-forward-loop transcriptional network promoting leukemic cell growth. Proc Natl Acad Sci U S A. 2006;103(48):18261-18266.
8. Weng AP, Millholland JM, Yashiro-Ohtani Y, et al. c-Myc is an important direct target of Notch1 in T-cell acute lymphoblastic leukemia/lymphoma. Genes Dev. 2006;20(15):2096-2109.
9. Vermezovic J, Adamowicz M, Santarpia L, et al. Notch is a direct negative regulator of the DNA-damage response. Nat Struct Mol Biol. 2015;22(5):417-424.
10. Di Veroli GY, Fornari C, Wang D, et al. Combenefit: an interactive platform for the analysis and visualization of drug combinations. Bioinformatics. 2016;32(18):2866-2868.
11. Li X, Gounari F, Protopopov A, Khazaie K, von Boehmer H. Oncogenesis of T-ALL and nonmalignant consequences of overexpressing intracellular NOTCH1. J Exp Med 2008;205(12):2851-2861.
12. Sanda T, Li X, Gutierrez A, et al. Interconnecting molecular pathways in the pathogenesis and drug sensitivity of T-cell acute lymphoblastic leukemia. Blood. 2010;115(9):1735-1745.
13. Ng OH, Erbilgin Y, Firtina S, et al. Deregulated WNT signaling in childhood T-cell acute lymphoblastic leukemia. Blood Cancer J. 2014;4(3):e192.
14. Van Vlierberghe P, Ambesi-Impiombato A, Perez-Garcia A, et al. ETV6 mutations in early immature human T cell leukemias. J Exp Med. 2011;208(13):2571-2579.
15. Thandapani P, Kloetgen A, Witkowski MT, et al. Valine tRNA levels and availability regulate complex I assembly in leukaemia. Nature. 2022;601(7893):428-433.
16. Liu Y, Easton J, Shao Y, et al. The genomic landscape of pediatric and young adult T-lineage acute lymphoblastic leukemia. Nat Genet. 2017;49(8):1211-1218.
17. Gutierrez A, Sanda T, Grebliunaite R, et al. High frequency of PTEN, PI3K, and AKT abnormalities in T-cell acute lymphoblastic leukemia. Blood. 2009;114(3):647-650.
18. Chen B, Jiang L, Zhong ML, et al. Identification of fusion genes and characterization of transcriptome features in T-cell acute lymphoblastic leukemia. Proc Natl Acad Sci U S A. 2018;115(2):373-378.
19. Agnusdei V, Minuzzo S, Frasson C, et al. Therapeutic antibody targeting of Notch1 in T-acute lymphoblastic leukemia xenografts. Leukemia. 2014;28(2):278-288.
20. Bordin F, Piovan E, Masiero E, et al. WT1 loss attenuates the TP53-induced DNA damage response in T-cell acute lymphoblastic leukemia. Haematologica. 2018;103(2):266-277.
21. Saccomani V, Grassi A, Piovan E, et al. miR-22-3p negatively affects tumor progression in T-cell acute lymphoblastic leukemia. Cells. 2020;9(7):1726.
22. Ngondo-Mbongo RP, Myslinski E, Aster JC, Carbon P. Modulation of gene expression via overlapping binding sites exerted by ZNF143, Notch1 and THAP11. Nucleic Acids Res. 2013;41(7):4000-4014.
23. Lehal R, Zaric J, Vigolo M, et al. Pharmacological disruption of the Notch transcription factor complex. Proc Natl Acad Sci U S A. 2020;117(28):16292-16301.
24. Winter GE, Mayer A, Buckley DL, et al. BET bromodomain proteins function as master transcription elongation factors independent of CDK9 recruitment. Mol Cell. 2017;67(1):5-18.
25. Lodi F, Certo M, Elkafrawy H, et al. BCAT1 inhibition affects CD8+ T cell activation, exhaustion, and tumoral immunity by altering iron homeostasis. bioRxiv. 2023 Feb 26. doi: 10.1101/2023.02.25.530034 [preprint not peer-reviewed].
26. Ko JH, Olona A, Papathanassiu AE, et al. BCAT1 affects mitochondrial metabolism independently of leucine transamination in activated human macrophages. J Cell Sci. 2020;133(22):jcs247957.
27. Shimazu T, Hirschey MD, Newman J, et al. Suppression of oxidative stress by beta-hydroxybutyrate, an endogenous histone deacetylase inhibitor. Science. 2013;339(6116):211-214.
28. Francois L, Boskovic P, Knerr J, et al. BCAT1 redox function maintains mitotic fidelity. Cell Rep. 2022;41(3):111524.
29. Fabbri G, Rasi S, Rossi D, et al. Analysis of the chronic lymphocytic leukemia coding genome: role of NOTCH1 mutational activation. J Exp Med. 2011;208(7):1389-1401.
30. Fabbri G, Holmes AB, Viganotti M, et al. Common nonmutational NOTCH1 activation in chronic lymphocytic leukemia. Proc Natl Acad Sci U S A. 2017;114(14):E2911-E2919.
31. Herold T, Jurinovic V, Metzeler KH, et al. An eight-gene expression signature for the prediction of survival and time to treatment in chronic lymphocytic leukemia. Leukemia. 2011;25(10):1639-1645.
32. Ananieva EA, Powell JD, Hutson SM. Leucine metabolism in T cell activation: mTOR signaling and beyond. Adv Nutr. 2016;7(4):798S-805S.
33. Hillier J, Allcott GJ, Guest LA, et al. The BCAT1 CXXC motif provides protection against ROS in acute myeloid leukaemia cells. Antioxidants (Basel). 2022;11(4):683.
34. Harris M, El Hindy M, Usmari-Moraes M, et al. BCAT-induced autophagy regulates Abeta load through an interdependence of redox state and PKC phosphorylation-implications in Alzheimer's disease. Free Radic Biol Med. 2020;152:755-766.
35. Rodrigues LM, Uribe-Lewis S, Madhu B, Honess DJ, Stubbs M, Griffiths JR. The action of beta-hydroxybutyrate on the growth, metabolism and global histone H3 acetylation of spontaneous mouse mammary tumours: evidence of a beta-hydroxybutyrate paradox. Cancer Metab. 2017;5:4.
36. Rojas-Morales P, Pedraza-Chaverri J, Tapia E. Ketone bodies, stress response, and redox homeostasis. Redox Biol. 2020;29:101395.
37. Ananieva EA, Wilkinson AC. Branched-chain amino acid metabolism in cancer. Curr Opin Clin Nutr Metab Care. 2018;21(1):64-70.
38. Luo L, Sun W, Zhu W, et al. BCAT1 decreases the sensitivity of cancer cells to cisplatin by regulating mTOR-mediated

autophagy via branched-chain amino acid metabolism. Cell Death Dis. 2021;12(2):169.
39. Chen CS, Wang YC, Yang HC, et al. Histone deacetylase inhibitors sensitize prostate cancer cells to agents that produce DNA double-strand breaks by targeting Ku70 acetylation. Cancer Res. 2007;67(11):5318-5327.
40. Hada M, Kwok RP. Regulation of ku70-bax complex in cells. J Cell Death. 2014;7:11-13.